

Quantum Circuit Design for Objective Function Maximization in Gate-Model Quantum Computers

Laszlo Gyongyosi*

Sandor Imre†

Abstract

Gate-model quantum computers provide an experimentally implementable architecture for near term quantum computations. To design a reduced quantum circuit that can simulate a high complexity reference quantum circuit, an optimization should be taken on the number of input quantum states, on the unitary operations of the quantum circuit, and on the number of output measurement rounds. Besides the optimization of the physical layout of the hardware layer, the quantum computer should also solve difficult computational problems very efficiently. To yield a desired output system, a particular objective function associated with the computational problem fed into the quantum computer should be maximized. The reduced gate structure should be able to produce the maximized value of the objective function. These parallel requirements must be satisfied simultaneously, which makes the optimization difficult. Here, we demonstrate a method for designing quantum circuits for gate-model quantum computers and define the Quantum Triple Annealing Minimization (QTAM) algorithm. The aim of QTAM is to determine an optimal reduced topology for the quantum circuits in the hardware layer at the maximization of the objective function of an arbitrary computational problem.

1 Introduction

According to Moore's law [39], traditional computer architectures will reach their physical limits in the near future. Quantum computers [4–13, 15–27] provide a tool to solve problems more efficiently than ever would be possible with traditional computers [4–13, 19]. The power of quantum computing is based on the fundamentals of quantum mechanics. In a quantum computer, information is represented by quantum information, and information processing is achieved by quantum gates that realize quantum operations [4–13, 19, 28–30]. These quantum operations are performed on the quantum states, which are then outputted and measured in a measurement phase. The measurement process is applied to each quantum state where the quantum information conveyed by the quantum states is converted into classical bits. Quantum computers have been demonstrated in practice [4–11], and several implementations are currently in progress [4–13, 19–23].

*School of Electronics and Computer Science, University of Southampton, Southampton SO17 1BJ, U.K., and Department of Networked Systems and Services, Budapest University of Technology and Economics, 1117 Budapest, Hungary, and MTA-BME Information Systems Research Group, Hungarian Academy of Sciences, 1051 Budapest, Hungary.

†Department of Networked Systems and Services, Budapest University of Technology and Economics, 1117 Budapest, Hungary.

In the physical layer of a gate-model quantum computer, the device contains quantum gates, quantum ports (of quantum gates), and quantum wires for the quantum circuit¹. In contrast to traditional automated circuit design [31–33, 35–38], a quantum system cannot participate in more than one quantum gate simultaneously. As a corollary, the quantum gates of a quantum circuit are applied in several rounds in the physical layer of the quantum circuit [4–13, 19–23].

The physical layout design and optimization of quantum circuits have different requirements with several open questions and currently represent an active area of study [4–13, 19–23]. Assuming that the goal is to construct a reduced quantum circuit that can simulate the original system, the reduction process should be taken on the number of input quantum states, gate operations of the quantum circuit, and the number of output measurements. Another important question is the maximization of objective function associated with an arbitrary computational problem that is fed into the quantum computer. These parallel requirements must be satisfied simultaneously, which makes the optimization procedure difficult and is an emerging issue in present and future quantum computer developments.

In the proposed QTAM method, the goal is to determine a topology for the quantum circuits of quantum computer architectures that can solve arbitrary computational problems such that the quantum circuit is minimized in the physical layer, and the objective function of an arbitrary selected computational problem is maximized. The physical layer minimization covers the simultaneous minimization of the quantum circuit area (quantum circuit height and depth of the quantum gate structure, where the depth refers to the number of time steps required for the quantum operations making up the circuit to be run on quantum hardware), the total area of the quantum wires of the quantum circuit, the maximization of the objective function, and the minimization of the required number of input quantum systems and output measurements. An important aim of the physical layout minimization is that the resulting quantum circuit should be identical to a high complexity reference quantum circuit (i.e., the reduced quantum circuit should be able to simulate a nonreduced quantum circuit).

The minimization of the total quantum wire length in the physical layout is also an objective in QTAM. It serves to improve the processing in the topology of the quantum circuit. However, besides the minimization of the physical layout of the quantum circuit, the quantum computer also has to solve difficult computational problems very efficiently (such as the maximization of an arbitrary combinatorial optimization objective function [20–23]). To achieve this goal in the QTAM method, we also defined an objective function that provides the maximization of objective functions of arbitrary computational problems. The optimization method can be further tuned by specific input constraints on the topology of the quantum circuit (paths in the quantum circuit, organization of quantum gates, required number of rounds of quantum gates, required number of measurement operators, Hamiltonian minimization, entanglement between quantum states, etc.) or other hardware restrictions of quantum computers, such as the well-known *no-cloning theorem* [26]. The various restrictions on quantum hardware, such as the number of rounds required to be integrated into the quantum gate structure, or entanglement generation between the quantum states are included in the scheme. These constraints and design attributes can be handled in the scheme through the definition of arbitrary constraints on the topology of the quantum circuit, or by constraints on the computational paths.

¹The term “quantum circuit”, in general, refers to software, not hardware; it is a description or prescription for what quantum operations should be applied when and does not refer to a physically implemented circuit analogous to a printed electronic circuit. In our setting, it refers to the hardware layer.

The combinatorial objective function is measured on a computational basis, and an objective function value is determined from the measurement result to quantify the current state of the quantum computer. Quantum computers can be used for combinatorial optimization problems. These procedures aim to use the quantum computer to produce a quantum system that is dominated by computational basis states such that a particular objective function is maximized.

Recent experimental realizations of quantum computers are qubit architectures [4–13, 15–23], and the current quantum hardware approaches focus on qubit systems (i.e., the dimension d of the quantum system is two, $d = 2$). However, while the qubit layout is straightforwardly inspirable by ongoing experiments, the method is developed for arbitrary dimensions to make it applicable for future implementations. Motivated by these assumptions, we therefore would avoid the term ‘qubit’ in our scheme to address the quantum states and instead use the generalized term, ‘quantum states’ throughout, which refers to an arbitrary dimensional quantum system. We also illustrate the results through superconducting quantum circuits [4–8]; however, the framework is general and flexible, allowing a realization for near term gate-model quantum computer implementations.

The novel contributions of this paper are as follows:

- *We define a method for designing quantum circuits for gate-model quantum computers.*
- *We conceive the QTAM algorithm, which provides a quantum circuit minimization on the physical layout (circuit depth and area), quantum wire length minimization, objective function maximization, input size and measurement size minimization for quantum circuits.*
- *We define a multilayer structure for quantum computations using the hardware restrictions on the topology of gate-model quantum computers.*

This paper is organized as follows. In Section 2 the related works are summarized. Section 3 proposes the system model. In Section 4 the details of the optimization method are discussed, while Section 5 studies the performance of the model. Finally, Section 6 concludes the paper. Supplemental information is included in the Appendix.

2 Related Works

The related works are summarized as follows.

A strong theoretical background on the logical model of gate-model quantum computers can be found in [20–22]. In [19], the model of a gate-model quantum neural network model is defined.

In [40], the authors defined a hierarchical approach to computer-aided design of quantum circuits. The proposed model was designed for the synthesis of permutation class of quantum logic circuits. The method integrates evolutionary and genetic approaches to evolve arbitrary quantum circuit specified by a target unitary matrix. Instead of circuit optimization, the work focuses on circuit synthesis.

In [41], the authors propose a simulation of quantum circuits by low-rank stabilizer decompositions. The work focuses on the problem of simulation of quantum circuits containing a few non-Clifford gates. The framework focuses on the theoretical description of the stabilizer rank. The authors also derived the simulation cost.

A method for the designing of a T-count optimized quantum circuit for integer multiplication with $4n + 1$ qubits was defined in [42]. The T-count [43] measures the number of T-gates, and has a relevance because of the implementation cost of a T gate is high. The aim of the T-count

optimization is to reduce the number of T-gates without substantially increasing the number of qubits. The method also applied for quantum circuit designs of integer division [44]. In the optimization takes into consideration both the T-count and T-depth, since T-depth is also an important performance measure to reduce the implementation costs. Another method for designing of reversible floating point divider units was proposed in [45].

In [46], a methodology for quantum logic gate construction was defined. The main purpose of the scheme was to construct fault-tolerant quantum logic gates with a simple technique. The method is based on the quantum teleportation method [47].

A method for the synthesis of depth-optimal quantum circuits was defined in [48]. The aim of the proposed algorithm is to compute the depth-optimal decompositions of logical operations via an application of the so-called meet-in-the-middle technique. The authors also applied their scheme for the factorizations of some quantum logical operations into elementary gates in the Clifford+T set.

A framework to the study the compilation and description of fault-tolerant, high level quantum circuits is proposed in [49]. The authors defined a method to convert high level quantum circuits consisting of commonly used gates into a form employing all decompositions and ancillary protocols needed for fault-tolerant error correction. The method also represents a useful tool for quantum hardware architectures with topological quantum codes.

The Quantum Approximate Optimization Algorithm (QAOA) optimization algorithm is defined in [21]. The QAOA has been defined to evaluate approximate solutions for combinatorial optimization problems fed into the quantum computer.

Relevant attributes of the QAOA algorithm are studied in [50].

In [51], the authors analyzed the performance of the QAOA algorithm on near-term gate-model quantum devices.

The implementation of QAOA with parallelizable gates is studied in [52].

In [53] the performance of QAOA is studied on different problems. The analysis covers the MaxCut combinatorial optimization problem, and the problem of quantum circuit optimizations on a classical computer using automatic differentiation and stochastic gradient descent. The work also revealed that QAOA can exceed the performance of a classical polynomial time algorithm (Goemans-Williamson algorithm [56]) with modest circuit depth. The work also concluded that the performance of QAOA with fixed circuit depth is insensitive to problem size.

In [54], the authors studied the problem of ultrafast state preparation via the QAOA with long range interactions. The work provides an application for the QAOA in near-term gate-model quantum devices. As the authors concluded, the QAOA-based approach leads to an extremely efficient state preparation, for example the method allows us to prepare Greene-Horne-Zeilinger (GHZ) states with $\mathcal{O}(1)$ circuit depth. The results were also demonstrated by several other examples.

Another experimental approach for the implementation of qubit entanglement and parallel logic operations with a superconducting circuit was presented in [55]. In this work, the authors generated entangled GHZ states with up to 10 qubits connecting to a bus resonator in a superconducting circuit. In the proposed implementation, the resonator-mediated qubit-qubit interactions are used to control the entanglement between the qubits and to operate on different pairs in parallel.

A review on the noisy intermediate-scale quantum (NISQ) era can be found in [1].

The subject of quantum computational supremacy is discussed in [2,3].

For a survey on the attributes of quantum channels, see [13], a survey on quantum computing technology is included in [14].

3 System Model

The simultaneous physical-layer minimization and the maximization of the objective function are achieved by the Quantum Triple Annealing Minimization (QTAM) algorithm. The QTAM algorithm utilizes the framework of simulated annealing (SA) [31–33, 35–38], which is a stochastic point-to-point search method.

The procedure of the QTAM algorithm with the objective functions are depicted in Fig. 1. The detailed descriptions of the methods and procedures are included in the next sections.

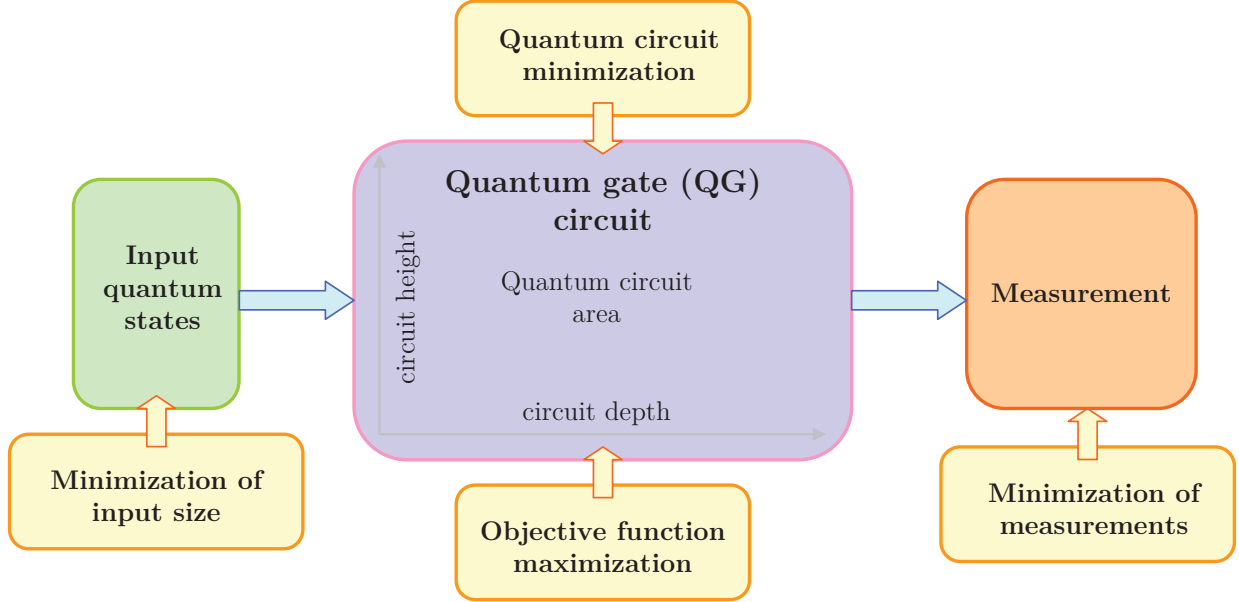


Figure 1: The QTAM method for quantum computers. The quantum gate (QG) circuit computation model consists of an input array of n quantum states (depicted by the green box), layers of quantum gates integrated into a quantum circuit (depicted by the purple box), and a measurement phase (depicted by the orange box). The quantum gates that act on the quantum states formulate a quantum circuit with a given circuit height and depth. The area of the quantum circuit is minimized by objective function F_1 , while the total quantum wire area of the quantum circuit is minimized by F_2 ($F_1 \wedge F_2$ is referred via the quantum circuit minimization). The result of the minimization is a quantum circuit of quantum gates with minimized quantum circuit area, minimized total quantum wire length, and a minimized total Hamiltonian operator. The maximization of a corresponding objective function of arbitrary selected computational problems for the quantum computer is achieved by F_3 (referred via the objective function maximization). Objective functions F_4 and F_5 are defined for the minimization of the number of quantum states (minimization of input size), and the total number of measurements (minimization of measurements).

3.1 Computational Model

By theory, in an SA-based procedure a current solution s_A is moved to a neighbor s_B , which yields an acceptance probability [31–33, 35–38]

$$\Pr(f(s_A), f(s_B)) = \frac{1}{1 + e^{\left(\frac{f(s_A) - f(s_B)}{Tf(s_A)}\right)}}, \quad (1)$$

where $f(s_A)$ and $f(s_B)$ represent the relative performances of the current and neighbor solutions, while T is a control parameter, $T(t) = T_{\max} \exp(-R(t/k))$, where R is the temperature decreasing rate, t is the iteration counter, k is a scaling factor, while T_{\max} is an initial temperature.

Since SA is a probabilistic procedure it is important to minimize the acceptance probability of unfavorable solutions and avoid getting stuck in a local minima.

Without loss of generality, if T is low, (1) can be rewritten in function of $f(s_A)$ and $f(s_B)$ as

$$\Pr(f(s_A), f(s_B)) = \begin{cases} 1, & \text{if } f(s_A) > f(s_B) \\ 0, & \text{if } f(s_A) \leq f(s_B) \end{cases}. \quad (2)$$

In the QTAM algorithm, we take into consideration that the objectives, constraints, and other functions of the method, by some fundamental theory, are characterized by different magnitude ranges [31–33, 35–38]. To avoid issues from these differences in the QTAM algorithm we define three annealing temperatures, $T_f(t)$ for objectives, $T_g(t)$ for constraints and $T_c(t)$ for the probability distribution closeness (distance of the output distributions of the reference quantum circuit and the reduced quantum circuit).

In the QTAM algorithm, the acceptance probability of a new solution s_B at a current solution s_A is as

$$\Pr(s_A, s_B) = \frac{1}{1 + e^{\tilde{d}(f)T_f(t)} e^{\tilde{d}(g)T_g(t)} e^{\tilde{d}(c)T_c(t)}}, \quad (3)$$

where $\tilde{d}(f)$, $\tilde{d}(g)$ and $\tilde{d}(c)$ are the average values of objective, constraint and distribution closeness domination, see Algorithm 1.

To aim of the QTAM algorithm is to minimize the cost function

$$\min f(x) = \alpha_1 F_1(x) + \dots + \alpha_{N_{obj}} F_{N_{obj}}(x) + F_s, \quad (4)$$

where x is the vector of design variables, while α is the vector of weights, while N_{obj} is the number of primarily objectives. Other i secondary objectives (aspect ratio of the quantum circuit, overlaps, total net length, etc.) are minimized simultaneously via the single-objective function F_s in (4) as

$$F_s = \sum_i \alpha_i F_i(x). \quad (5)$$

3.2 Objective Functions

We defined $N_{obj} = 5$ objective functions for the QTAM algorithm. Objective functions F_1 and F_2 are defined for minimization of QG quantum circuit in the physical layer. The aim of objective function F_1 is the minimization of the A_{QG} quantum circuit area of the QG quantum gate structure,

$$F_1 : \min(A_{QG}) = \min(H'_{QG} \cdot D'_{QG}), \quad (6)$$

where H'_{QG} is the optimal circuit height of QG , while D'_{QG} is the optimal depth of QG .

Focusing on superconducting quantum circuits [4–8], the aim of F_2 is the physical layout minimization of the w_{QG} total quantum wire area of QG , as

$$F_2 : w_{QG} = \min \sum_{k=1}^h \left(\sum_{i=1}^p \sum_{j=1}^q \ell_{ij} \cdot \delta_{ij} (\psi_{ij}) \right), \quad (7)$$

where h is the number of nets of the QG circuit, p is the number of quantum ports of the QG quantum circuit considered as sources of a condensate wave function amplitude [4–8], and q the number of quantum ports considered as sinks of a condensate wave function amplitude, ℓ_{ij} is the length of the quantum wire ij , δ_{ij} is the effective width of the quantum wire ij , while ψ_{ij} is the (root mean square) condensate wave function amplitude [4–8] associated to the quantum wire ij .

Objective function F_3 is defined for the maximization of the expected value of an objective function $C_L(\vec{\Phi})$ as

$$F_3 : \max C_L(\vec{\Phi}) = \max \langle \vec{\Phi} | C | \vec{\Phi} \rangle, \quad (8)$$

where C is an objective function, $\vec{\Phi}$ is a collection of L parameters

$$\vec{\Phi} = \Phi_1, \dots, \Phi_L \quad (9)$$

such that with L unitary operations, state $|\vec{\Phi}\rangle$ is evaluated as

$$|\vec{\Phi}\rangle = U_L(\Phi_L), \dots, U_1(\Phi_1) |\varphi\rangle, \quad (10)$$

where U_i is an i -th unitary that depends on a set of parameters Φ_i , while $|\varphi\rangle$ is an initial state. Thus the goal of F_3 is to determine the L parameters of $\vec{\Phi}$ (see (9)) such that $\langle \vec{\Phi} | C | \vec{\Phi} \rangle$ is maximized.

Objective functions F_4 and F_5 are defined for the minimization of the number of input quantum states and the number of required measurements. The aim of objective function F_4 is the minimization of the number of quantum systems on the input of the QG circuit,

$$F_4 : \min(n). \quad (11)$$

The aim of objective function F_5 is the minimization of the total number of measurements in the M measurement block,

$$F_5 : \min(m) = \min(N_M |M|), \quad (12)$$

where $m = N_M |M|$, where N_M is the number of measurement rounds, $|M|$ is the number of measurement gates in the M measurement block.

3.3 Constraint Violations

The optimization at several different objective functions results in different Pareto fronts [31–33,35] of placements of quantum gates in the physical layout. These Pareto fronts allow us to find feasible tradeoffs between the optimization objectives of the QTAM method. The optimization process includes diverse objective functions, constraints, and optimization criteria to improve the performance of the quantum circuit and to take into consideration the hardware restrictions of quantum computers. In the proposed QTAM algorithm the constraints are endorsed by the modification of the Pareto dominance [31–33,35] values by the different sums of constraint violation values. We defined three different constraint violation values.

3.3.1 Distribution Closeness Dominance

In the QTAM algorithm, the Pareto dominance is first modified with the sum of distribution closeness violation values, denoted by $c_s(\cdot)$. The aim of this iteration is to support the closeness of output distributions of the reduced quantum circuit QG to the output distribution of the reference quantum circuit QG_R .

Let P_{QG_R} the output distribution after the M measurement phase of the reference (original) quantum circuit QG_R to be simulated by QG , and let Q_{QG} be the output distribution of the actual, reduced quantum circuit QG . The distance between the quantum circuit output distributions P_{QG_R} and Q_{QG} (distribution closeness) is straightforwardly yielded by the relative entropy function, as

$$D(P_{QG_R} \| Q_{QG}) = \sum_i P_{QG_R}(i) \log_2 \frac{P_{QG_R}(i)}{Q_{QG}(i)}. \quad (13)$$

For two solutions x and y , the $d_{x,y}(c)$ distribution closeness dominance function is defined as

$$d_{x,y}(c) = c_s(x) - c_s(y), \quad (14)$$

where $c_s(\cdot)$ is evaluated for a given solution z as

$$c_s(z) = \sum_{i=1}^{N_v} v_i^c, \quad (15)$$

where v_i^c is an i -th distribution closeness violation value, N_v is the number of distribution closeness violation values for a solution z .

In terms of distribution closeness dominance, x dominates y if the following relation holds:

$$\begin{aligned} & ((c_s(x) < 0) \wedge (c_s(y) < 0) \wedge (c_s(x) > c_s(y))) \\ & \vee ((c_s(x) = 0) \wedge (c_s(y) < 0)), \end{aligned} \quad (16)$$

thus (16) states that x dominates y if both x and y are unfeasible, and x is closer to feasibility than y , or x is feasible and y is unfeasible.

By similar assumptions, y dominates x if

$$\begin{aligned} & ((c_s(x) < 0) \wedge (c_s(y) < 0) \wedge (c_s(x) < c_s(y))) \\ & \vee ((c_s(x) < 0) \wedge (c_s(y) = 0)). \end{aligned} \quad (17)$$

3.3.2 Constraint Dominance

The second modification of the Pareto dominance is by the sum of constraint violation values,

$$d_{x,y}(g) = g_s(x) - g_s(y), \quad (18)$$

where $g_s(\cdot)$ is the sum of all constraint violation values, evaluated for a given solution z as

$$g_s(z) = \sum_{i=1}^{N_g} v_i^g, \quad (19)$$

where v_i^g is an i -th constraint violation value, N_g is the number of constraint violation values for a solution z .

Similar to (16) and (17), in terms of constraint dominance, x dominates y if the following relation holds:

$$\begin{aligned} & ((g_s(x) < 0) \wedge (g_s(y) < 0) \wedge (g_s(x) > g_s(y))) \\ & \vee ((g_s(x) = 0) \wedge (g_s(y) < 0)), \end{aligned} \quad (20)$$

thus (16) states that x dominates y if both x and y are unfeasible, and x is closer to feasibility than y , or x is feasible and y is unfeasible.

By similar assumptions, y dominates x with respect to $g_s(\cdot)$ if

$$\begin{aligned} & ((g_s(x) < 0) \wedge (g_s(y) < 0) \wedge (g_s(x) < g_s(y))) \\ & \vee ((g_s(x) < 0) \wedge (g_s(y) = 0)). \end{aligned} \quad (21)$$

3.3.3 Objective Dominance

Let x and y refer to two solutions, then, by theory, the $d_{x,y}(f)$ objective dominance function is defined as

$$d_{x,y}(f) = \prod_{i=1, f_1(x) \neq f_1(y)}^{N_{obj}} \frac{|f_i(x) - f_i(y)|}{R_i}, \quad (22)$$

where N_{obj} is the number of objectives (in our setting $N_{obj} = 5$), R_i is the range of objective i , while x dominates y if $f_i(x) \leq f_i(y)$ for $\forall_i = 1, \dots, N_{obj}$, and for at least one i the relation $f_i(x) < f_i(y)$ holds.

3.4 Objective Function Maximization

The quantum circuit QG executes operations in the \mathcal{H} Hilbert space. The dimension of the \mathcal{H} space is

$$\dim(\mathcal{H}) = d^n, \quad (23)$$

where d is the dimension of the quantum system ($d = 2$ for a qubit system), while n is the number of quantum states.

Using the formalism of [20–22], let assume that the computational problem fed into the quantum circuit QG is specified by n bits and m constraints. Then, the objective function is defined as

$$C(z) = \sum_{\alpha=1}^m C_{\alpha}(z), \quad (24)$$

where

$$z = z_1 \dots z_n \quad (25)$$

is an n -length bitstring, and $C_{\alpha}(z) = 1$ if z satisfies constraint α , and $C_{\alpha}(z) = 0$ otherwise [20–22].

Assuming a Hilbert space of n qubits, $\dim(\mathcal{H}) = 2^n$, using the computational basis vectors $|z\rangle$, operator $C(z)$ in (24) is a diagonal operator in the computational basis [20–22]. Then, at a particular angle γ , $\gamma \in [0, \pi]$, unitary $U(C, \gamma)$ is evaluated as

$$U(C, \gamma) = e^{-i\gamma C} = \prod_{\alpha=1}^m e^{-i\gamma C_{\alpha}}, \quad (26)$$

such that all terms in the product are diagonal in the computational basis.

Then, for the μ dependent product of commuting operators, $\mu \in [0, \pi]$ [20–22], a unitary $U(B, \mu)$ is defined as

$$U(B, \mu) = e^{-i\mu B} = \prod_{j=1}^n e^{-i\mu \sigma_x^j}, \quad (27)$$

where $B = \sum_i X_i$, $X_i = \sigma_x^i$, σ_x is the Pauli X -operator, while μ is a control parameter [20–23], $\mu \in [0, \pi]$. For a qubit setting, the $|s\rangle$ initial state of the quantum computer is the uniform superposition over computational basis states,

$$|s\rangle = \frac{1}{\sqrt{2^n}} \sum_z |z\rangle. \quad (28)$$

Let assume that the $G_{QG}^{k,r}$ multilayer structure of the QG quantum circuit contains n quantum ports of several quantum gates, and edge set

$$\mathcal{S}_E = \{\langle jk \rangle\} \quad (29)$$

of size m . Then, the aim of the optimization is to indentify a string z (25) that the maximizes the objective function

$$C = \sum_{\langle jk \rangle} C_{\langle jk \rangle}, \quad (30)$$

where

$$C_{\langle jk \rangle} = \frac{1}{2} (1 - z_i z_j), \quad (31)$$

where $z_i = \pm 1$.

In $G_{QG}^{k,r}$ different unitary operations can be defined for the single quantum ports (qubits) and the connected quantum ports, as follows.

Let $U_{q_s}(\mu_j)$ be a unitary operator on a q_s single port (qubits) in $G_{QG}^{k,r}$, be defined such that for each quantum ports a μ_j parameter is associated as

$$U_{q_s}(\mu_j) = e^{-i\mu_j X_j}. \quad (32)$$

For the collection

$$\vec{\mu} = (\mu_1, \dots, \mu_n), \quad (33)$$

the resulting unitary is

$$U_{q_s}(\vec{\mu}) = \prod_j U_{q_s}(\mu_j). \quad (34)$$

The unitary $U_{q_s}(\vec{\mu})$ is therefore represents the applications of the unitary operations at once in the quantum ports of the QG quantum circuit.

Then, let unitary $U_{q_{jk}}(\gamma_{jk})$ be defined for connected quantum ports q_{jk} in $G_{QG}^{k,r}$, as

$$U_{q_{jk}}(\gamma_{jk}) = e^{i\gamma_{jk} Z_j Z_k}, \quad (35)$$

where $Z_i = \sigma_z^i$, where σ_z is the Pauli Z -operator. Since the eigenvalues of X_i and $Z_j Z_k$ are ± 1 , it allows us to restrict the values [20–22] of parameters γ and μ to the range of $[0, \pi]$.

Then, defining collection

$$\vec{\gamma} = (\gamma_{jk}^1, \dots, \gamma_{jk}^h), \quad (36)$$

where h is the number of individual γ_{jk} parameters, the unitary $U_{q_{jk}}(\vec{\gamma})$ is yielded as

$$U_{q_{jk}}(\vec{\gamma}) = \prod_{\langle jk \rangle \in G_{QG}^{k,r}} U_{q_{jk}}(\gamma_{jk}). \quad (37)$$

Assuming that there exists a set $\mathcal{S}_{\vec{\mu}}^u$ of u collections of $\vec{\mu}$'s

$$\mathcal{S}_{\vec{\mu}}^u : \vec{\mu}^{(1)}, \dots, \vec{\mu}^{(u)} \quad (38)$$

and a set $\mathcal{S}_{\vec{\gamma}}^u$ of u collections of $\vec{\gamma}$'s,

$$\mathcal{S}_{\vec{\gamma}}^u : \vec{\gamma}^{(1)}, \dots, \vec{\gamma}^{(u)}, \quad (39)$$

a $|\phi\rangle$ system state of the QG quantum circuit is evaluated as

$$\begin{aligned} |\phi\rangle &= |\mathcal{S}_{\vec{\mu}}^u, \mathcal{S}_{\vec{\gamma}}^u, C\rangle \\ &= U_{q_s}(\vec{\mu}^{(u)}) U_{q_{jk}}(\vec{\gamma}^{(u)}) \dots U_{q_s}(\vec{\mu}^{(1)}) U_{q_{jk}}(\vec{\gamma}^{(1)}) |s\rangle, \end{aligned} \quad (40)$$

where $|s\rangle$ is given in (28).

The maximization of objective function (24) in the multilayer $G_{QG}^{k,r}$ structure is therefore analogous to the problem of finding the parameters of sets $\mathcal{S}_{\vec{\mu}}^u$ (38) and $\mathcal{S}_{\vec{\gamma}}^u$ (39) in the system state $|\phi\rangle$ (40) of the QG quantum circuit.

3.5 The QTAM Algorithm

Theorem 1 *The QTAM algorithm utilizes annealing temperatures $T_f(t)$, $T_g(t)$ and $T_c(t)$ to evaluate the acceptance probabilities, where $T_f(t)$ is the annealing temperature for the objectives, $T_g(t)$ is the annealing temperature for the constraints and $T_c(t)$ is the annealing temperature for the distribution closeness.*

Proof. The detailed description of the QTAM procedure is given in Algorithm 1.

The related steps are detailed in Sub-procedures 1-4. In Step 3 of Sub-procedure 1, the best \mathcal{A}_s solutions refer to those solutions from \mathcal{A} that have the largest values of the crowding distance [35]. Particularly, in this step, the solutions are also sorted and compared by a crowded comparison operator to find the best solution.

■

3.5.1 Computational Complexity of QTAM

Following the complexity analysis of [31–33, 35], the computational complexity of QTAM is evaluated as

$$\mathcal{O}(N_d N_{it} |\mathcal{P}| (N_{obj} + \log_2(|\mathcal{P}|))), \quad (54)$$

where N_d is the number of dominance measures, N_{it} is the number of total iterations, $|\mathcal{P}|$ is the population size, while N_{obj} is the number of objectives.

Algorithm 1 *Quantum Triple Annealing Minimization (QTAM)*

Step 1. Define an archive \mathcal{A} with random solutions, and select a ξ random solution from \mathcal{A} .

Step 2. Define ν as $\nu = \Xi(\xi)$, where $\Xi(\cdot)$ is a moving operator. Determine the dominance relation between ξ and ν via $\mathcal{D}_P(\xi, \nu)$, where function $\mathcal{D}_P(\cdot)$ is the constrained Pareto dominance checking function.

Step 3. Evaluate acceptance probabilities based on $\mathcal{D}_P(\xi, \nu)$.

(a): If $\mathcal{D}_P(\xi, \nu) = \nu \angle \xi$ (ξ dominates ν , where \angle is the Pareto dominance operator), then $\xi = \nu$, with probability

$$\Pr(\xi = \nu | \nu \angle \xi) = \frac{1}{1 + e^{\tilde{d}(f)T_f(t)} e^{\tilde{d}(g)T_g(t)} e^{\tilde{d}(c)T_c(t)}}, \quad (41)$$

where $\tilde{d}(f)$, is the average objective dominance, evaluated as

$$\tilde{d}(f) = \frac{\left(\sum_{i=1}^k d_{i,\nu}(f)\right) + d_{\xi,\nu}(f)}{k+1}, \quad (42)$$

where $d_{x,y}(f)$ is the objective dominance function as given in (22), while $\tilde{d}(g)$ average constraint dominance as

$$\tilde{d}(g) = \frac{-\left(\sum_{i=1}^k d_{\nu,i}(g)\right) - d_{\nu,\xi}(g)}{k+1}, \quad (43)$$

where $d_{x,y}(g)$ is the constraint dominance function as given in (18), and $\tilde{d}(c)$ is average distribution closeness dominance as

$$\tilde{d}(c) = \frac{-\left(\sum_{i=1}^k d_{\nu,i}(c)\right) - d_{\nu,\xi}(c)}{k+1}, \quad (44)$$

where $d_{x,y}(c)$ is the distribution closeness dominance function as given in (14), while $T_f(t)$ is the annealing temperature for the objectives

$$T_f(t) = T_{f_{\max}} e^{-R\left(\frac{t}{k}\right)}, \quad (45)$$

where R is the temperature decreasing rate, $T_{f_{\max}}$ is a maximum (initial) value for annealing the objectives factor, $T_g(t)$ is the annealing temperature for the constraints

$$T_g(t) = T_{g_{\max}} e^{-R\left(\frac{t}{k}\right)}, \quad (46)$$

where $T_{g_{\max}}$ is a maximum (initial) value for annealing the constraint factor, and $T_c(t)$ is the annealing temperature for the distribution closeness

$$T_c(t) = T_{c_{\max}} e^{-R\left(\frac{t}{k}\right)}, \quad (47)$$

where $T_{c_{\max}}$ is a maximum (initial) value for annealing the distribution closeness factor, respectively.

Algorithm 1 *Quantum Triple Annealing Minimization (QTAM), cont.*

(b). If $\mathcal{D}_P(\xi, \nu) = (\nu \neg \angle \xi) \wedge (\xi \neg \angle \nu)$ (ν and ξ are non-dominating to each other) such that ν is dominated by $k \geq 1$ points in \mathcal{A} , $\mathcal{D}_P(\xi, \nu) = \nu \angle (\mathcal{A})_k$, then $\xi = \nu$, with probability

$$\begin{aligned} & \Pr(\xi = \nu | (\nu \neg \angle \xi) \wedge (\xi \neg \angle \nu), \nu \angle (\mathcal{A})_k) \\ &= \frac{1}{1 + e^{\tilde{d}(f)_k T_f(t)} e^{\tilde{d}(g)_k T_g(t)} e^{\tilde{d}(c)_k T_c(t)}}, \end{aligned} \quad (48)$$

where

$$\tilde{d}(f)_k = \tilde{d}(f) - d_{\xi, \nu}(f), \quad (49)$$

where $\tilde{d}(f)$ is as in (42),

$$\tilde{d}(g)_k = \tilde{d}(g) + d_{\nu, \xi}(g), \quad (50)$$

where $\tilde{d}(g)$ is as in (43), while

$$\tilde{d}(c)_k = \tilde{d}(c) + d_{\nu, \xi}(c), \quad (51)$$

where $\tilde{d}(c)$ is as in (44).

(c): If $\mathcal{D}_P(\xi, \nu) = (\nu \neg \angle \xi) \wedge (\xi \neg \angle \nu)$, and $\mathcal{D}_P(\nu, \mathcal{A}) = (\mathcal{A} \neg \angle \nu)$, thus ν is non-dominating with respect to \mathcal{A} , then apply Sub-procedure 1.

(d): If $\mathcal{D}_P(\xi, \nu) = (\nu \neg \angle \xi) \wedge (\xi \neg \angle \nu)$, and $\mathcal{D}_P(\nu, \mathcal{A}) = ((\mathcal{A})_k \angle \nu)$, thus ν dominates $k \geq 1$ points in \mathcal{A} , then apply Sub-procedure 2.

(e): If $\mathcal{D}_P(\xi, \nu) = \xi \angle \nu$ such that $\mathcal{D}_P(\nu, \mathcal{A}) = (\nu \angle (\mathcal{A})_k)$, thus ν is dominated by $k \geq 1$ points in \mathcal{A} , then set $\xi = \nu$, with probability

$$\Pr(\xi = \nu | \xi \angle \nu, \nu \angle (\mathcal{A})_k) = \frac{1}{1 + e^{-\tilde{d}(\min)}}, \quad (52)$$

where $\tilde{d}(\min)$ is evaluated as

$$\tilde{d}(\min) = \min_{\forall k} (d_{\nu, k}(f) - (d_{k, \nu}(g) + d_{k, \nu}(c))). \quad (53)$$

Using (53), apply Sub-procedure 3. To evaluate the $\mathcal{D}_P(\nu, \mathcal{A})$ relations between ν and the elements of \mathcal{A} at $\mathcal{D}_P(\xi, \nu) = \xi \angle \nu$, apply Sub-procedure 4.

Step 4. Apply Steps 2-3, until $i < N_{it}$, where i is the actual iteration, N_{it} is the total number of iterations.

Sub-procedure 1

Step 1. Set $\xi = \nu$, and add ν to \mathcal{A} .

Step 2. If $|\mathcal{A}| > A_s$, where $|\mathcal{A}|$ is the number of elements in \mathcal{A} , A_s is the maximal archive size, then assign $\Delta_{cr}(\mathcal{A})$ to \mathcal{A} , where $\Delta_{cr}(\cdot)$ is the crowding distance.

Step 3. Select the best A_s elements.

Sub-procedure 2

Step 1. Set $\xi = \nu$, and add ν to \mathcal{A} .

Step 2. Remove all the k dominated points from \mathcal{A} .

Sub-procedure 3

Step 1. Set $\xi = k_{\tilde{d}(\min)}$, where $k_{\tilde{d}(\min)}$ is a point of \mathcal{A} that corresponds to $\tilde{d}(\min)$ (see (53)) with probability $\Pr(\xi = \nu | \xi \angle \nu, \nu \angle (\mathcal{A})_k)$ (see (52)).

Step 2. Otherwise set $\xi = \nu$.

Sub-procedure 4

Step 1. If $\mathcal{D}_P(\nu, \mathcal{A}) = \mathcal{A} \neg \angle \nu$, i.e., ν is non-dominating with respect to \mathcal{A} , then set $\xi = \nu$, and add ν to \mathcal{A} . If $|\mathcal{A}| > A_s$, then assign $\Delta_{cr}(\mathcal{A})$ to \mathcal{A} , and select the best A_s elements.

Step 2. If $\mathcal{D}_P(\nu, (\mathcal{A})_k) = (\mathcal{A})_k \angle \nu$, i.e., ν dominates k points in \mathcal{A} , then set $\xi = \nu$, and add ν to \mathcal{A} . Remove the k points from \mathcal{A} .

4 Wiring Optimization and Objective Function Maximization

4.1 Multilayer Quantum Circuit Grid

An i -th quantum gate of QG is denoted by g_i , a k -th port of the quantum gate g_i is referred to as $g_{i,k}$. Due to the hardware restrictions of gate-model quantum computer implementations [20–23], the quantum gates are applied in several rounds. Thus, a multilayer, k -dimensional (for simplicity we assume $k = 2$), n -sized finite square-lattice grid $G_{QG}^{k,r}$ can be constructed for QG , where r is the number of layers, $l_z, z = 1, \dots, r$. A quantum gate g_i in the z -th layer l_z is referred to as $g_i^{l_z}$, while a k -th port of $g_i^{l_z}$ is referred to as $g_{i,k}^{l_z}$.

4.2 Method

Theorem 2 *There exists a method for the parallel optimization of quantum wiring in physical-layout of the quantum circuit and for the maximization of an objective function $C_\alpha(z)$.*

Proof. The aim of this procedure (Method 1) is to provide a simultaneous physical-layer optimization and Hamiltonian minimization via the minimization of the wiring lengths in the multilayer structure of QG and the maximization of the objective function (see also Section 3.4). Formally, the aim of Method 1 is the $F_2 \wedge F_3$ simultaneous realization of the objective functions F_2 and F_3 .

Using the $G_{QG}^{k,r}$ multilayer grid of the QG quantum circuit determined via F_1 and F_2 , the aim of F_3 maximization of the objective function $C(z)$, where $z = z_1 \dots z_n$ in an n -length input string, where each z_i is associated to an edge of $G_{QG}^{k,r}$ connecting two quantum ports. The objective function $C(z)$ associated to an arbitrary computational problem is defined as

$$C(z) = \sum_{\langle i,j \rangle \in G_{QG}^{k,r}} C_{\langle i,j \rangle}(z), \quad (55)$$

where $C_{\langle i,j \rangle}$ is the objective function for an edge of $G_{QG}^{k,r}$ that connects quantum ports i and j .

The $C^*(z)$ maximization of objective function (55) yields a system state Ψ for the quantum computer [20–23] as

$$\Psi = \langle \gamma, \mu, C^*(z) | C^*(z) | \gamma, \mu, C^*(z) \rangle, \quad (56)$$

where

$$| \gamma, \mu, C^*(z) \rangle = U(B, \mu) U(C^*(z), \gamma) |s\rangle, \quad (57)$$

while

$$U(C^*(z), \gamma) |z\rangle = e^{-i\gamma C^*(z)} |z\rangle, \quad (58)$$

where γ is a single parameter [20–23].

The objective function (55) without loss of generality can be rewritten as

$$C(z) = \sum_{\alpha} C_{\alpha}(z), \quad (59)$$

where C_{α} each act on a subset of bits, such that $C_{\alpha} \in \{0, 1\}$. Therefore, there exists a selection of parameters of $\vec{\Phi}$ in (9) such that (59) picks up a maximized value $C^*(z)$, which yields system state Υ as

$$\Upsilon = \langle \vec{\Phi} | C^*(z) | \vec{\Phi} \rangle. \quad (60)$$

Therefore, the resulting Hamiltonian H associated to the system state (60) is minimized via F_2 (see (72)) as

$$E_L(\vec{\Phi}) = \min \langle \vec{\Phi} | H | \vec{\Phi} \rangle, \quad (61)$$

since the physical-layer optimization minimizes the ℓ_{ij} physical distance between the quantum ports, therefore the energy $E_L(\vec{\Phi})$ of the Hamiltonian associated to $\vec{\Phi}$ is reduced to a minima.

The steps of the method $F_2 \wedge F_3$ are given in Method 1. The method minimizes the number of quantum wires in the physical-layout of QG , and also achieves the desired system state Ψ of (56).

■

The steps of Method 1 are illustrated in Fig. 2, using the $G_{QG}^{k,r}$ multilayer topology of the QG quantum gate structure, l_i refers to the i -th layer of $G_{QG}^{k,r}$.

4.3 Quantum Circuit Minimization

For objective function F_1 , the area minimization of the QG quantum circuit requires the following constraints. Let $S_v(P_i)$ be the vertical symmetry axis of a proximity group P_i [31–33] on QG , and let $x_{S_v(P_i)}$ refer to the x -coordinate of $S_v(P_i)$. Then, by some symmetry considerations for $x_{S_v(P_i)}$,

$$x_{S_v(P_i)} = \frac{1}{2} (x_i^1 + x_i^2 + \kappa_i), \quad (62)$$

where x_i is the bottom-left x coordinate of a cell σ_i , κ_i is the width of σ_i , and

$$y_i^1 + \frac{h_i}{2} = y_i^2 + \frac{h_i}{2}, \quad (63)$$

where y_i is the bottom-left y coordinate of a cell σ_i , h_i is the height of σ_i .

Method 1 *Quantum Wiring Optimization and Objective Function Maximization*

Step 1. Construct the $G_{QG}^{k,r}$ multilayer grid of the QG quantum circuit, with r layers l_1, \dots, l_r . Determine the

$$C(z) = \sum_{\langle i,j \rangle \in G_{QG}^{k,r}} C_{\langle i,j \rangle}(z)$$

objective function, where each $C_{\langle i,j \rangle}$ refers to the objective function for an edge in $G_{QG}^{k,r}$ connecting quantum ports i and j , defined as

$$C_{\langle i,j \rangle}(z) = \frac{1}{2}(1 - z_i z_j),$$

where $z_i = \pm 1$.

Step 2. Find the optimal assignment of separation point Δ in $G_{QG}^{k,r} = (V, E, f)$ at a physical-layer blockage β via a minimum-cost tree in $G_{QG}^{k,r}$ containing at least one port from each quantum gate g_i , $i = 1, \dots, |V|$. For all pairs of quantum gates g_i, g_j , minimize the $f_{p,c}$ path cost (L1 distance) between a source quantum gate g_i and destination quantum gate g_j and then maximize the overlapped L1 distance between g_i and Δ .

Step 3. For the s found assignments of Δ in Step 2, evaluate the objective functions C_{α_i} , $k = 1, \dots, s$, where C_{α_0} is the initial value. Let the two paths \mathcal{P}_1 and \mathcal{P}_2 between quantum ports $g_{i,1}, g_{j,1}, g_{j,2}$ be given as $\mathcal{P}_1 : g_{i,1} \rightarrow \Delta \rightarrow g_{j,1}$, and $\mathcal{P}_2 : g_{i,1} \rightarrow \Delta \rightarrow g_{j,2}$. Evaluate objective functions $C_{\langle g_{i,1}, \Delta \rangle}(z)$, $C_{\langle \Delta, g_{j,1} \rangle}(z)$ and $C_{\langle \Delta, g_{j,2} \rangle}(z)$.

Step 4. Select that k -th solution, for which

$$C_{\alpha_k}(z) = C_{\langle g_{i,1}, \Delta \rangle}^{(k)}(z) + C_{\langle \Delta, g_{j,1} \rangle}^{(k)}(z) + C_{\langle \Delta, g_{j,2} \rangle}^{(k)}(z)$$

is maximal, where $C_{\langle i,j \rangle}^{(k)}$ is the objective function associated to a k -th solution between quantum ports $g_{i,1}, g_{j,1}$, and $g_{i,1}, g_{j,2}$ in $G_{QG}^{k,r}$. The resulting $C_{\alpha}^*(z)$ for \mathcal{P}_1 and \mathcal{P}_2 is as

$$C_{\alpha}^*(z) = \max_k (C_{\alpha_k}(z)).$$

Step 5. Repeat steps 2-4 for all paths of $G_{QG}^{k,r}$.

Let (σ^1, σ^2) be a symmetry pair [31–33] that refers to two matched cells placed symmetrically in relation to $S_v(P_i)$, with bottom-left coordinates $(\sigma^1, \sigma^2) = ((x_i^1, y_i^1), (x_i^2, y_i^2))$. Then, $x_{S_v(P_i)}$ can be rewritten as

$$x_{S_v(P_i)} = x_i^1 - x_i = x_i^2 + x_i + \kappa_i, \quad (64)$$

with the relation $y_i^1 = y_i^2 = y_i$.

Let $\sigma^S = (x_i^S, y_i^S)$ be a cell which is placed centered [31–33] with respect to $S_v(P_i)$. Then, $x_{S_v(P_i)}$ can be evaluated as

$$x_{S_v(P_i)} = x_i^S + \frac{\kappa_i}{2}, \quad (65)$$

along with $y_i^S = y_i$. Note that it is also possible that for some cells in QG there is no symmetry requirements, these cells are denoted by σ^0 .

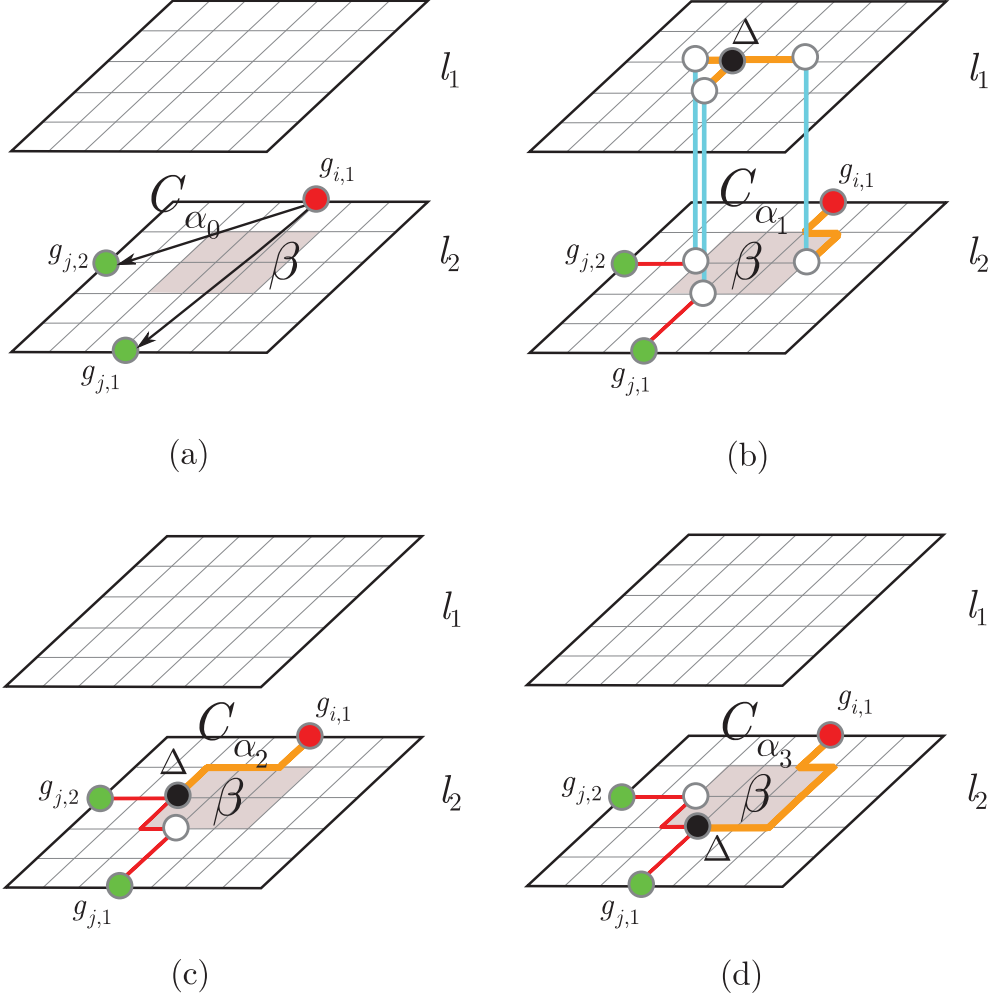


Figure 2: The aim is to find the optimal wiring in $G_{QG}^{k,r}$ for the QG quantum circuit (minimal path length with maximal overlapped path between $g_{i,1}$ and $g_{j,1}, g_{j,2}$) such that the C_α objective function associated to the paths $\mathcal{P}_1 : g_{i,1} \rightarrow g_{j,1}$, and $\mathcal{P}_2 : g_{i,1} \rightarrow g_{j,2}$ is maximal. (a): The initial objective function value is C_{α_0} . A physical-layer blockage β in the quantum circuit allows no to use paths \mathcal{P}_1 and \mathcal{P}_2 . (b): The wire length is optimized via the selection point Δ . The path cost is $f_{p,c} = 11 + 3f_l$, where f_l is the cost function of the path between the layers l_1 and l_2 (depicted by the blue vertical line), the path overlap from $g_{i,1}$ to Δ is $\tau_o = 5 + f_l$. The objective function value is C_{α_1} . (c): The path cost is $f_{p,c} = 10$, the path overlap from $g_{i,1}$ to Δ is $\tau_o = 4$. The objective function value is C_{α_2} . (d): The path cost is $f_{p,c} = 12$, the path overlap from $g_{i,1}$ to Δ is $\tau_o = 6$. The objective function value is C_{α_3} . The selected connection topology from (b), (c), and (d) is that which yields the maximized objective function C_α^* .

As can be concluded, using objective function F_1 for the physical-layer minimization of QG , a

d -dimensional constraint vector $\mathbf{x}_{F_1}^d$ can be formulated with the symmetry considerations as follows:

$$\mathbf{x}_{F_1}^d = \sum_{N_{(\sigma^1, \sigma^2)}} (x_i, y_i, r_i) + \sum_{N_{\sigma^S}} (y_i, r_i) + \sum_{N_{\sigma^0}} (x_i, y_i, r_i), \quad (66)$$

where $N_{(\sigma^1, \sigma^2)}$ is the number of (σ^1, σ^2) symmetry pairs, N_{σ^S} is the number of σ^S -type cells, while N_{σ^0} is the number of σ^0 -type cells, while r_i is the rotation angle of an i -th cell σ_i , respectively.

4.3.1 Quantum Wire Area Minimization

Objective function F_2 provides a minimization of the total quantum wire length of the QG circuit. To achieve it we define a procedure that yields the minimized total quantum wire area, w_{QG} , of QG as given by (7). Let δ_{ij} be the effective width of the quantum wire ij in the QG circuit, defined as

$$\delta_{ij} = \frac{\psi_{ij}}{J_{\max}(T_{ref}) h_{nom}}, \quad (67)$$

where ψ_{ij} is the (root mean square) condensate wave function amplitude, $J_{\max}(T_{ref})$ is the maximum allowed current density at a given reference temperature T_{ref} , while h_{nom} is the nominal layer height. Since drops in the condensate wave function phase φ_{ij} are also could present in the QG circuit environment, the δ'_{ij} effective width of the quantum wire ij can be rewritten as

$$\delta'_{ij} = \frac{\psi_{ij} \ell_{eff} r_0 (T_{ref})}{\chi_{\varphi_{ij}}}, \quad (68)$$

where $\chi_{\varphi_{ij}}$ is a maximally allowed value for the phase drops, ℓ_{eff} is the effective length of the quantum wire, $\ell_{eff} \leq (\chi_{\varphi_{ij}} \delta_{ij}) / \psi_{ij} r_0 (T_{ref})$, while $r_0 (T_{ref})$ is a conductor sheet resistance [4–8].

In a $G_{QG}^{k,r}$ multilayer topological representation of QG , the ℓ_{ij} distance between the quantum ports is as

$$\ell_{ij} = |x_i - x_j| + |y_i - y_j| + |z_i - z_j| f_l, \quad (69)$$

where f_l is a cost function between the layers of the multilayer structure of QG .

During the evaluation, let $w_{QG}(k)$ be the total quantum wire area of a particular net k of the QG circuit,

$$w_{QG}(k) = \sum_{i=1}^p \sum_{j=1}^q \ell_{ij} \cdot \delta_{ij}(\psi_{ij}), \quad (70)$$

where q quantum ports are considered as sources of condensate wave function amplitudes, while p of QG are sinks, thus (7) can be rewritten as

$$F_2 : w_{QG} = \min \sum_{k=1}^h w_{QG}(k). \quad (71)$$

Since ψ_{ij} is proportional to $\delta_{ij}(\psi_{ij})$, (71) can be simplified as

$$F_2 : w'_{QG} = \min \sum_{k=1}^h w'_{QG}(k), \quad (72)$$

where

$$w'_{QG}(k) = \sum_{i=1}^p \sum_{j=1}^q \ell_{ij} \cdot \psi_{ij}, \quad (73)$$

where ℓ_{ij} is given in (69).

In all quantum ports of a particular net k of QG , the source quantum ports are denoted by positive sign [31–33] in the condensate wave function amplitude, ψ_{ij} assigned to quantum wire ij between quantum ports i and j , while the sink ports are depicted by negative sign in the condensate wave function amplitude, $-\psi_{ij}$ with respect to a quantum wire ij between quantum ports i and j .

Thus the aim of $w_{QG}(k)$ in (70) is to determine a set of port-to-port connections in the QG quantum circuit, such that the number of long connections is reduced in a particular net k of QG as much as possible. The result in (71) is therefore extends these requirements for all nets of QG .

Wave Function Amplitudes With respect to a particular quantum wire ij between quantum ports i and j of QG , let $\psi_{i \rightarrow j}$ refer to the condensate wave function amplitude in direction $i \rightarrow j$, and let $\psi_{j \rightarrow i}$ refer to the condensate wave function amplitude in direction $j \rightarrow i$ in the quantum circuit. Then, let be ϕ_{ij} defined for the condensate wave function amplitudes of quantum wire ij as

$$\phi_{ij} = \min(|\psi_{i \rightarrow j}|, |\psi_{j \rightarrow i}|), \quad (74)$$

with a residual condensate wave function amplitude

$$\xi_{i \rightarrow j} = \phi_{ij} - \psi_{i \rightarrow j}, \quad (75)$$

where $\psi_{i \rightarrow j}$ is an actual amplitude in the forward direction $i \rightarrow j$. Thus, the maximum amount of condensate wave function amplitude injectable to of quantum wire ij in the forward direction $i \rightarrow j$ at the presence of $\psi_{i \rightarrow j}$ is $\xi_{i \rightarrow j}$ (see (75)). The following relations holds for a backward direction, $j \rightarrow i$, for the decrement of a current wave function amplitude $\psi_{i \rightarrow j}$ as

$$\bar{\xi}_{j \rightarrow i} = -\psi_{i \rightarrow j}, \quad (76)$$

with residual quantum wire length

$$\Gamma_{j \rightarrow i} = -\delta_{ij}, \quad (77)$$

where δ_{ij} is given in (67).

By some fundamental assumptions, the \mathcal{N}_R residual network of QG is therefore a network of the quantum circuit with forward edges for the increment of the wave function amplitude ψ , and backward edges for the decrement of ψ . To avoid the problem of negative wire lengths the Bellman-Ford algorithm [31–33] can be utilized in an iterative manner in the residual directed graph of the QG topology.

To find a path between all pairs of quantum gates in the directed graph of the QG quantum circuit, the directed graph has to be strongly connected. The strong-connectivity of the h nets with the parallel minimization of the connections of the QG topology can be achieved by a minimum spanning tree method such as Kruskal's algorithm [31–33].

Lemma 1 *The objective function F_2 is feasible in a multilayer QG quantum circuit structure.*

Proof. The procedure defined for the realization of objective function F_2 on a QG quantum circuit is summarized in Method 2. The proof assumes a superconducting architecture.

The sub-procedures of Method 2 are detailed in Sub-methods 2.1, 2.2 and 2.3.

These conclude the proof. ■

Method 2 *Implementation of Objective Function F_2*

- Step 1.** Assign the ψ_{ij} condensate wave function amplitudes for all ij quantum wires of QG via Sub-method 2.1.
- Step 2.** Determine the residual network of QG via Sub-method 2.2.
- Step 3.** Achieve the strong connectivity of QG via Sub-method 2.3.
- Step 4.** Output the QG quantum circuit topology such that w_{QG} (7) is minimized.
-

Sub-method 2. 1

- Step 1.** Create a M_{QG} multilayer topological map of the network \mathcal{N} of QG with the quantum gates and ports.
- Step 2.** From M_{QG} determine the L_c connection list of \mathcal{N} in QG .
- Step 3.** Determine the δ_{ij} the effective width of the quantum wire ij via (67), for $\forall ij$ wires.
- Step 4.** Determine ϕ_{ij} via (74) for all quantum wires ij of the QG circuit.
- Step 5.** For a k -th net of QG , assign the wave function amplitude values ψ_{ij} to $\forall ij$ quantum wires such that $w_{QG}(k)$ in (70) is minimized, with quantum wire length ℓ_{ij} (69).
-

Sub-method 2. 2

- Step 1.** Create a \bar{M}_{QG} multilayer topological map of the \mathcal{N}_R residual network of QG .
- Step 2.** From \bar{M}_{QG} determine the \bar{L}_c connection list of the \mathcal{N}_R residual network of QG .
- Step 3.** For $\forall i \rightarrow j$ forward edges of \bar{M}_{QG} of \mathcal{N}_R , compute the $\xi_{i \rightarrow j}$ residual condensate wave function amplitude (75), and for $\forall j \rightarrow i$ backward edges of \bar{M}_{QG} , compute the quantity $\bar{\xi}_{j \rightarrow i}$ via (76).
- Step 4.** Compute the residual negative quantum wire length $\Gamma_{j \rightarrow i}$ via (77), using δ_{ij} from (67).
- Step 5.** Determine the \bar{C} negative cycles in the \bar{M}_{QG} of the \mathcal{N}_R residual network of QG via the \mathcal{A}_{BF} Bellman-Ford algorithm [31–33].
- Step 6.** If $N_{\bar{C}} > 0$, where $N_{\bar{C}}$ is the number of \bar{C} negative cycles in \bar{M}_{QG} , then update the ψ_{ij} wave function amplitudes of the quantum wires ij in the to cancel out the negative cycles.
- Step 7.** Re-calculate the values of (75), (76) and (77) for the residual edges of \mathcal{N}_R .
- Step 8.** Repeat steps 5-7, until $N_{\bar{C}} > 0$.
-

4.3.2 Processing in the Multilayer Structure

The $G_{QG}^{k,z}$ grid consists of all g_i quantum gates of QG in a multilayer structure, such that the $g_{i,k}^{l_z}$ appropriate ports of the quantum gates are associated via an directed graph $G = (V, E, f_c)$, where V is the set of ports, $g_{i,k}^{l_z} \subseteq V$, E is the set of edges, and f_c is a cost function, to achieve the gate-to-gate connectivity.

As a hardware restriction we use a constraint on the quantum gate structure, it is assumed in the model that a given quantum system cannot participate in more than one quantum gate at a particular time.

The distance in the rectilinear grid $G_{QG}^{k,z}$ of QG is measured by the $d_{L1}(\cdot)$ L1-distance function.

Sub-method 2. 3

- Step 1.** For an i -th $sn_{k,i}$ subnet of a net k of the QG quantum circuit, set the quantum wire length to zero, $\delta_{ij} = 0$ between quantum ports i and j , for all $\forall i$.
- Step 2.** Determine the $L2$ (Euclidean) distance between the quantum ports of the subnets $sn_{k,i}$ (from each quantum port of a subnet to each other quantum port of all remaining subnets [31]).
- Step 3.** Weight the $\delta_{ij} > 0$ non-zero quantum wire lengths by the calculated $L2$ distance between the connections of the subnets of the QG quantum circuit [4–8], [31–33].
- Step 4.** Determine the minimum spanning tree \mathcal{T}_{QG} via the \mathcal{A}_K Kruskal algorithm [31].
- Step 5.** Determine the set $S_{\mathcal{T}_{QG}}$ of quantum wires with $\delta_{ij} > 0$ from \mathcal{T}_{QG} . Calculate $\delta_{S_{\mathcal{T}_{QG}}} = \max(\delta_{ij}, \delta'_{ij}, \delta_0)$, where δ_0 is the minimum width can be manufactured, while δ_{ij} and δ'_{ij} are given in (67) and (68).
- Step 6.** Add the quantum wires of $S_{\mathcal{T}_{QG}}$ to the M_{QG} multilayer topological map of the network \mathcal{N} of QG .
- Step 7.** Repeat steps 4-6 for $\forall k$ nets of the QG quantum circuit, until M_{QG} is not strongly connected.
-

Between two network ports $x, y \in V$, $x = (j, k)$, $y = (m, o)$, $d_{L1}(\cdot)$ is as

$$d_{L1}(x, y) = d_{L1}((j, k), (m, o)) = |m - j| + |o - k|. \quad (78)$$

The quantum port selection in the $G_{QG}^{k,r}$ multilayer structure of QG , with r layers l_z , $z = 1, \dots, r$, and $k = 2$ dimension in each layers is illustrated in Fig. 3.

Algorithm

Theorem 3 *The Quantum Shortest Path Algorithm finds shortest paths in a multilayer QG quantum circuit structure.*

Proof. The steps of the shortest path determination between the ports of the quantum gates in a multilayer structure are included in Algorithm 2.

■

Complexity Analysis The complexity analysis of Algorithm 2 is as follows. Since the QSPA algorithm (Algorithm 2) is based on the A^* search method [31–33], the complexity is trivially yielded by the complexity of the A^* search algorithm.

5 Performance Evaluation

In this section, we compare the performance of the proposed QTAM method with a multiobjective evolutionary algorithm called NSGA-II [34]. We selected this multiobjective evolutionary algorithm for the comparison, since the method can be adjusted for circuit designing.

The computational complexity of NSGA-II is proven to be $\mathcal{O}(N_{it}N_{obj}|\mathcal{P}|^2)$ in general, while at an optimized nondominated procedure, the complexity can be reduced to $\mathcal{O}(N_{it}N_{obj}|\mathcal{P}|\log_2|\mathcal{P}|)$.

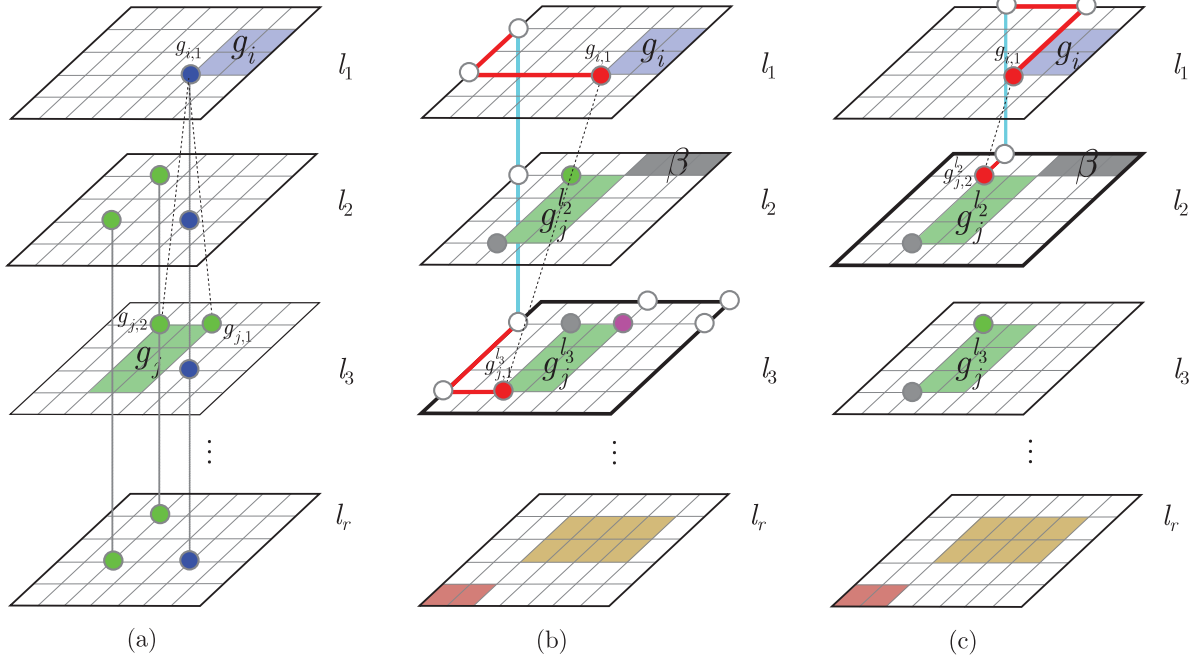


Figure 3: The method of port allocation of the quantum gates in the $G_{QG}^{k,r}$ multilayer structure, with r layers $l_z, z = 1, \dots, r$, and $k = 2$ dimension in each layers. The aim of the multiport selection is to find the shortest path between ports of quantum gates g_i (blue rectangle) and g_j (green rectangle) in the $G_{QG}^{2,r}$ multilayer structure. (a): The quantum ports needed to be connected in QG are port $g_{i,1}$ in quantum gate g_i in layer l_1 , and ports $g_{j,1}$ and $g_{j,2}$ of quantum gate g_j in layer l_3 . (b): Due to a hardware restriction on quantum computers, the quantum gates are applied in several rounds in the different layers of the quantum circuit QG . Quantum gate g_j is applied in two rounds in two different layers that is depicted $g_j^{l_3}$ and $g_j^{l_2}$. For the layer- l_3 quantum gate $g_j^{l_3}$, the active port is $g_{j,1}^{l_3}$ (red), while the other port is not accessible (gray) in l_3 . The $g_{j,1}^{l_3}$ port, due to a physical-layer blockage β in the quantum circuit of the above layer l_2 does not allow to minimize the path cost between ports $g_{i,1}$ and $g_{j,1}^{l_3}$. The target port $g_{j,1}^{l_3}$ is therefore referred to as a blocked port (depicted by pink), and a new port of is $g_j^{l_3}$ selected for $g_{j,1}^{l_3}$ (new port depicted by red). (c): For the layer- l_2 quantum gate $g_j^{l_2}$, the active port is $g_{j,2}^{l_2}$ (red), while the remaining port is not available (gray) in l_2 . The white dots (vertices) represent auxiliary ports in the grid structure of the quantum circuit. In $G_{QG}^{2,r}$, each vertices could have a maximum of 8 neighbors, thus for a given port $g_{j,k}$ of a quantum gate g_j , $\deg(g_{j,k}) \leq 8$.

Algorithm 2 *Quantum Shortest Path Algorithm (QSPA)*

Step 1. Create the $G_{QG}^{k,r}$ multilayer structure of QG , with r layers l_z , $z = 1, \dots, r$, and k dimension in each layers. From $G_{QG}^{k,r}$ generate a list $L_{\mathcal{P} \in QG}$ of the paths between each start quantum gate port to each end quantum gate port in the $G_{QG}^{k,r}$ structure of QG quantum circuit.

Step 2. Due to the hardware restrictions of quantum computers, add the decomposed quantum gate port information and its layer information to $L_{\mathcal{P} \in QG}$. Add the β physical-layer blockage information to $L_{\mathcal{P} \in QG}$.

Step 3. For a quantum port pair $(x, y) \in G_{QG}^{k,r}$ define the $f_c(x, y)$ cost function, as

$$f_c(x, y) = \gamma(x, y) + d_{L1}(x, y),$$

where $\gamma(x, y)$ is the real path size from x to y in the multilayer grid structure $G_{QG}^{k,r}$ of QG , while $d_{L1}(x, y)$ is the L1 distance in the grid structure as given by (78).

Step 4. Using $L_{\mathcal{P} \in QG}$ and cost function $f_c(x, y)$, apply the A^* parallel search [31–33] to determine the lowest cost path $\mathcal{P}^*(x, y)$.

We take into consideration both situations for a comparison. The complexity of QTAM is given in (54).

The complexity of the methods in terms of the number of iterations, N_O , is compared in Fig. 4. The performance of QTAM is depicted in Fig. 4(a), while Fig. 4(b) and Fig. 4(c) illustrate the performances of the NSGA-II and optimized NSGA-II, respectively.

For the comparison, the N_{obj} parameter is set to $N_{obj} = 5$, while for the QTAM method, N_d is set to $N_d = 3$.

In the analyzed range, the maximized values of N_O are $N_O(\text{QTAM}) \approx 2 \cdot 10^6$, $N_O(\text{NSGA-II}) \approx 1.25 \cdot 10^8$, and for the optimized NSGA-II scenario, $N'_O(\text{NSGA-II}) \approx 2.25 \cdot 10^6$, respectively. In comparison to NSGA-II, the complexity of QTAM is significantly lower. Note, while the performance of QTAM and the optimized NSGA-II is closer, QTAM requires no any optimization of the complexity of the nondominated procedure.

6 Conclusions

The algorithms and methods presented here provide a framework for quantum circuit designs for near term gate-model quantum computers. Since our aim was to define a scheme for present and future quantum computers, the developed algorithms and methods were tailored for arbitrary-dimensional quantum systems and arbitrary quantum hardware restrictions. We demonstrated the results through gate-model quantum computer architectures; however, due to the flexibility of the scheme, arbitrary implementations and input constraints can be integrated into the quantum circuit minimization. The objective function that is the subject of the maximization in the method can also be selected arbitrarily. This allows a flexible implementation to solve any computational problem for experimental quantum computers with arbitrary hardware restrictions and development constraints.

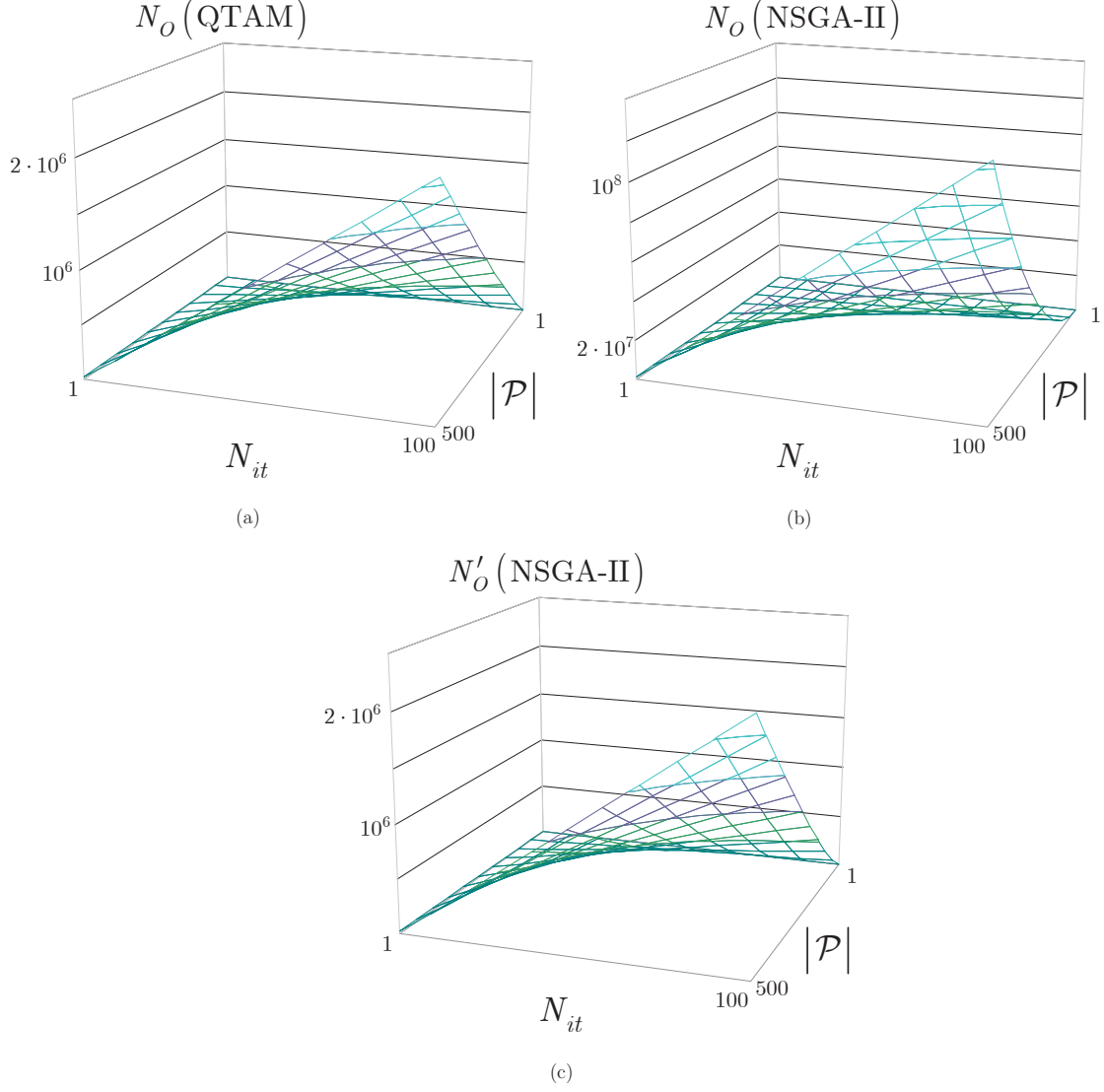


Figure 4: (a): The computational complexity (N_O : number of operations) of QTAM in function of N_{it} and $|\mathcal{P}|$, $N_{it} \in [1, 100]$, $|\mathcal{P}| \in [1, 500]$. (b): The computational complexity of the NSGA-II method in function of N_{it} and $|\mathcal{P}|$, $N_{it} \in [1, 100]$, $|\mathcal{P}| \in [1, 500]$. (c): The computational complexity of the optimized NSGA-II in function of N_{it} and $|\mathcal{P}|$, $N_{it} \in [1, 100]$, $|\mathcal{P}| \in [1, 500]$.

Acknowledgements

This work was partially supported by the European Research Council through the Advanced Fellow Grant, in part by the Royal Society’s Wolfson Research Merit Award, in part by the Engineering and Physical Sciences Research Council under Grant EP/L018659/1, by the Hungarian Scientific Research Fund - OTKA K-112125 and in part by the Engineering and Physical Sciences Research Council under Grant EP/L018659/1.

References

- [1] Preskill, J. Quantum Computing in the NISQ era and beyond, *Quantum* 2, 79 (2018).
- [2] Harrow, A. W. and Montanaro, A. Quantum Computational Supremacy, *Nature*, vol 549, pages 203-209 (2017).
- [3] Aaronson, S. and Chen, L. Complexity-theoretic foundations of quantum supremacy experiments. *Proceedings of the 32nd Computational Complexity Conference, CCC '17*, pages 22:1-22:67, (2017).
- [4] Ofek, N. et al. Extending the lifetime of a quantum bit with error correction in superconducting circuits. *Nature* 536, 441-445 (2016).
- [5] Debnath, S. et al. Demonstration of a small programmable quantum computer with atomic qubits. *Nature* 536, 63-66 (2016).
- [6] Barends, R. et al. Superconducting quantum circuits at the surface code threshold for fault tolerance. *Nature* 508, 500-503 (2014).
- [7] Monz, T. et al. Realization of a scalable Shor algorithm. *Science* 351, 1068-1070 (2016).
- [8] DiCarlo, L. et al. Demonstration of two-qubit algorithms with a superconducting quantum processor. *Nature* 460, 240-244 (2009).
- [9] Higgins, B. L., Berry, D. W., Bartlett, S. D., Wiseman, H. M. and Pryde, G. J. Entanglement-free Heisenberg-limited phase estimation. *Nature* 450, 393-396 (2007).
- [10] Vandersypen, L. M. K. et al. Experimental realization of Shor’s quantum factoring algorithm using nuclear magnetic resonance. *Nature* 414, 883-887 (2001).
- [11] Gulde, S. et al. Implementation of the Deutsch-Jozsa algorithm on an ion-trap quantum computer. *Nature* 421, 48-50 (2003).
- [12] IBM. *A new way of thinking: The IBM quantum experience*. URL: <http://www.research.ibm.com/quantum>. (2017).
- [13] Gyongyosi, L., Imre, S. and Nguyen, H. V. A Survey on Quantum Channel Capacities, *IEEE Communications Surveys and Tutorials* **99**, 1, doi: 10.1109/COMST.2017.2786748 (2018).
- [14] Gyongyosi, L. and Imre, S. A Survey on Quantum Computing Technology, *Computer Science Review*, Elsevier, DOI: 10.1016/j.cosrev.2018.11.002, ISSN: 1574-0137, (2018).

- [15] Biamonte, J. et al. Quantum Machine Learning. *Nature*, 549, 195-202 (2017).
- [16] Lloyd, S., Mohseni, M. and Rebentrost, P. Quantum principal component analysis. *Nature Physics*, 10, 631 (2014).
- [17] Sheng, Y. B., Zhou, L. Distributed secure quantum machine learning. *Science*, 62, 1025-2019 (2017).
- [18] Kimble, H. J. The quantum Internet. *Nature*, 453:1023-1030 (2008).
- [19] Farhi, E. and Neven, H. Classification with Quantum Neural Networks on Near Term Processors, *arXiv:1802.06002v1* (2018).
- [20] Farhi, E., Goldstone, J., Gutmann, S. and Neven, H. Quantum Algorithms for Fixed Qubit Architectures. *arXiv:1703.06199v1* (2017).
- [21] Farhi, E., Goldstone, J. and Gutmann, S. A Quantum Approximate Optimization Algorithm. *arXiv:1411.4028*. (2014).
- [22] Farhi, E., Goldstone, J. and Gutmann, S. A Quantum Approximate Optimization Algorithm Applied to a Bounded Occurrence Constraint Problem. *arXiv:1412.6062*. (2014).
- [23] Farhi, E. and Harrow, A. W. Quantum Supremacy through the Quantum Approximate Optimization Algorithm. *arxiv:1602.07674* (2016).
- [24] Lloyd, S., Shapiro, J. H., Wong, F. N. C., Kumar, P., Shahriar, S. M. and Yuen, H. P. Infrastructure for the quantum Internet. *ACM SIGCOMM Computer Communication Review*, 34, 9-20 (2004).
- [25] Van Meter, R. *Quantum Networking*, John Wiley and Sons Ltd, ISBN 1118648927, 9781118648926 (2014).
- [26] Gyongyosi, L. and Imre, S. *Advanced Quantum Communications - An Engineering Approach*. Wiley-IEEE Press (New Jersey, USA), (2012).
- [27] Lloyd, S. Mohseni, M. and Rebentrost, P. Quantum algorithms for supervised and unsupervised machine learning. *arXiv:1307.0411* (2013).
- [28] Pirandola, S., Laurenza, R., Ottaviani, C. and Banchi, L. Fundamental limits of repeaterless quantum communications, *Nature Communications*, 15043, doi:10.1038/ncomms15043 (2017).
- [29] Pirandola, S., Braunstein, S.L., Laurenza, R., Ottaviani, C., Cope, T.P.W., Spedalieri, G. and Banchi, L. Theory of channel simulation and bounds for private communication, *Quantum Sci. Technol.* 3, 035009 (2018).
- [30] Pirandola, S. Capacities of repeater-assisted quantum communications, *arXiv:1601.00966* (2016).
- [31] Martins, R., Lourenco, N. and Horta, N. *Analog Integrated Circuit Design Automation*, Springer, ISBN 978-3-319-34059-3, ISBN 978-3-319-34060-9 (2017).

- [32] Martins, R., Lourenco, N. and Horta, N. Multi-objective optimization of analog integrated circuit placement hierarchy in absolute coordinates. *Expert Syst. Appl.* 42(23), 9137–9151 (2015).
- [33] Martins, R., Pova, R., Lourenco, N. and Horta, N. Current-flow & current-density-aware multiobjective optimization of analog IC placement. *Integr. VLSI J.* (2016).
- [34] Deb, K., Pratap, A., Agarwal, S. and Meyarivan, T. A fast and elitist multiobjective genetic algorithm: NSGA-II, *IEEE Trans. Evol. Comput.*, vol. 6, no. 2, pp. 182–197, (2002).
- [35] Bandyopadhyay, S., Saha, S., Maulik, U. and Deb, K. A simulated annealing-based multiobjective optimization algorithm: AMOSA, *IEEE Trans. Evol. Comput.* 12(3), 269–283 (2008).
- [36] Suman, B. and Kumar, P. A survey of simulated annealing as a tool for single and multiobjective optimization. *J. Oper. Res. Soc.* 57, 1143–1160 (2006).
- [37] Jiang, I., Chang, H. Y. and Chang, C. L. WiT: Optimal wiring topology for electromigration avoidance, *IEEE Trans. Very Large Scale Integr. Syst.* 20(4), 581–592 (2012).
- [38] Rocha, F. A. E. R. M., Martins, F., Lourenco, N. C. C. and Horta, N. C. G. *Electronic Design Automation of Analog ICs, Combining Gradient Models with Multi-Objective Evolutionary Algorithms*, Springer (2014).
- [39] Moore, G. E. Cramming more components onto integrated circuits. *Electronics*. (1965).
- [40] Perkowski, M., Lukac, M., Kerntopf, P., Pivtoraiko, M., Folgheraiter, M., Choi, Y. W., Jungwook, K., Lee, D., Hwangbo, W. and Kim, H. A Hierarchical Approach to Computer-Aided Design of Quantum Circuits. *Electrical and Computer Engineering Faculty Publications and Presentations* 228. (2003).
- [41] Bravyi, S., Browne, D., Calpin, P., Campbell, E., Gosset, D. and Howard, M. Simulation of quantum circuits by low-rank stabilizer decompositions, arXiv:1808.00128 (2018).
- [42] Munoz-Coreas, E. and Thapliyal, H. Quantum Circuit Design of A T-count Optimized Integer Multiplier, *IEEE Transactions on Computers*, p 1-1, DOI: 10.1109/TC.2018.2882774 (2018).
- [43] Gosset, D., Kliuchnikov, V., Mosca, M. and Russo, V. An algorithm for the t-count, *Quantum Information and Computation*, vol. 14, no. 15-16, pp. 1261–1276, (2014).
- [44] Thapliyal, H., Munoz-Coreas, E., Varun, T. S. S. and Humble, T. S. Quantum Circuit Designs of Integer Division Optimizing T-count and T-depth, arXiv:1809.09732 (2018).
- [45] Jamal, L. and Babu, H. M. H. Efficient approaches to design a reversible floating point divider, in *2013 IEEE International Symposium on Circuits and Systems (ISCAS2013)*, pp. 3004–3007, (2013).
- [46] Zhou, X., Leung, D. W. and Chuang, I. L. Methodology for quantum logic gate construction, *Phys. Rev. A*, vol. 62, p. 052316 (2000).
- [47] Gottesman, D., Chuang, I. L. Quantum Teleportation is a Universal Computational Primitive, *Nature* 402, 390-393 (1999).

- [48] Amy, M., Maslov, D., Mosca, M. and Roetteler, M. A meet-in-the middle algorithm for fast synthesis of depth-optimal quantum circuits, *IEEE Transactions on Computer-Aided Design of Integrated Circuits and Systems*, vol. 32, no. 6, pp. 818–830, (2013).
- [49] Paler, A., Polian, I., Nemoto, K. and Devitt, S. J. Fault-tolerant, high level quantum circuits: form, compilation and description, *Quantum Science and Technology*, vol. 2, no. 2, p. 025003, (2017).
- [50] Brandao, F. G. S. L., Broughton, M., Farhi, E., Gutmann, S. and Neven, H. For Fixed Control Parameters the Quantum Approximate Optimization Algorithm’s Objective Function Value Concentrates for Typical Instances, *arXiv:1812.04170* (2018).
- [51] Zhou, L., Wang, S.-T., Choi, S., Pichler, H. and Lukin, M. D. Quantum Approximate Optimization Algorithm: Performance, Mechanism, and Implementation on Near-Term Devices, *arXiv:1812.01041* (2018).
- [52] Lechner, W. Quantum Approximate Optimization with Parallelizable Gates, *arXiv:1802.01157v2* (2018).
- [53] Gavin E. Crooks, Performance of the Quantum Approximate Optimization Algorithm on the Maximum Cut Problem, *arXiv:1811.08419* (2018).
- [54] Ho, W. W., Jonay, C. and Hsieh, T. H. Ultrafast State Preparation via the Quantum Approximate Optimization Algorithm with Long Range Interactions, *arXiv:1810.04817* (2018).
- [55] Song, C et al. 10-Qubit Entanglement and Parallel Logic Operations with a Superconducting Circuit, *Physical Review Letters*, vol. 119, no. 18, p. 180511 (2017).
- [56] Goemans, M. X. and Williamson, D. P. Improved approximation algorithms for maximum cut and satisfiability problems using semidefinite programming, *J. ACM* 42, 1115 (1995).

A Appendix

A.1 Abbreviations

EDA Electronic Design Automation

IC Integrated Circuit

QG Quantum Gate

QSPA Quantum Shortest Path Algorithm

QTAM Quantum Triple Annealing Minimization

SA Stimulated Annealing

VLSI Very-Large-Scale Integration

A.2 Notations

The notations of the manuscript are summarized in Table A.1.

Table A.1: Summary of notations.

<i>Notation</i>	<i>Description</i>
d	Dimension of the quantum system, $d = 2$ for a qubit system.
H	Hamiltonian operator.
QG	Reduced quantum circuit.
QG_R	Reference (non-reduced) quantum circuit.
P_{QG}	Output distribution of QG .
P_{QG_R}	Output distribution of QG_R .
n	Number of input quantum systems
F_i	An i -th objective function.
s	A solution.
$f(s)$	The relative performance of a solution s .
T	Control parameter in the SA method.
R	Temperature decreasing rate in SA.
t	Iteration counter for the SA method.
k	Scaling factor.
T_{\max}	Initial temperature in the SA framework.

$d(f), d(g), d(c)$	Objective, constraint and distribution closeness domination functions.
$\tilde{d}(f), \tilde{d}(g), \tilde{d}(c)$	Average values of objective, constraint and distribution closeness domination functions.
\mathbf{x}	A vector of design variables.
α	A vector of weights.
N_{obj}	Number of objectives in the optimization procedure.
F_s	A single-objective function.
A_{QG}	Quantum circuit area of the QG quantum gate structure.
H'_{QG}	Optimal circuit height of QG .
D'_{QG}	Optimal depth of QG .
w_{QG}	Total quantum wire area of QG .
h	Number of nets of the QG circuit.
p	Number of quantum ports of the QG quantum circuit considered as sources of a condensate wave function amplitude.
q	Number of quantum portsf considered as sinks of a condensate wave function amplitude.
ℓ_{ij}	Length of the quantum wire ij .
δ_{ij}	Effective width of the quantum wire ij .
ψ_{ij}	Condensate wave function amplitude associated to the quantum wire ij .
$\vec{\Phi}$	A collection of L parameters $\vec{\Phi} = \Phi_1, \dots, \Phi_L$.
$ \vec{\Phi}\rangle$	A system state of the quantum computer, $ \vec{\Phi}\rangle = U_L(\Phi_L), \dots, U_1(\Phi_1) \varphi\rangle$, where U_i is an i -th unitary that depends on a set of parameters Φ_i , while $ \varphi\rangle$ is an initial state.
m	Total number of measurements in the M measurement block, $m = N_M M $, where N_M is the number of measurement rounds, $ M $ is the number of measurement gates in the M measurement block.
$c_s(\cdot)$	Sum of distribution closeness violation values.
$D(\cdot \ \cdot)$	Relative entropy function.
$d_{x,y}(c)$	Distribution closeness dominance function for solutions x and y .
v_i^c	An i -th distribution closeness violation value.

N_v	The number of distribution closeness violation values for a solution z .
$g_s(\cdot)$	Sum of all constraint violation values.
v_i^g	An i -th constraint violation value.
N_g	Number of constraint violation values for a solution z .
$d_{x,y}(f)$	Objective dominance function.
R_i	Range of an objective i .
\mathcal{A}	Archive.
ξ	A random solution from \mathcal{A} .
ν	Parameter, $\nu = \Xi(\xi)$, where $\Xi(\cdot)$ is a moving operator.
$\mathcal{D}_P(\cdot)$	Constrained Pareto dominance checking function.
\angle	Pareto dominance operator; for $\nu \angle \xi$, ξ dominates ν .
N_{it}	Total number of iterations.
N_d	Number of dominance measures.
$ \mathcal{P} $	Population size.
N_{obj}	Number of objectives.
g_i	An i -th quantum gate of QG .
$g_{i,k}$	A k -th port of the quantum gate g_i of the quantum circuit.
$G_{QG}^{k,r}$	A multilayer, k -dimensional n -sized finite square-lattice base-graph rectilinear grid, where r is the number of layers, l_z , $z = 1, \dots, r$.
$g_i^{l_z}$	A quantum gate g_i in the z -th layer l_z of $G_{QG}^{k,r}$.
$g_{i,k}^{l_z}$	A k -th port of $g_i^{l_z}$ in $G_{QG}^{k,r}$.
$C(z)$	Objective function of a computational problem, z is a bitstring that encodes the state of the quantum circuit.
$C_{\langle i,j \rangle}$	Objective function for an edge of $G_{QG}^{k,r}$ that connects quantum ports i and j .
z_i	Parameter, $z_i = \pm 1$.
$C^*(z)$	Maximized objective function.
U	Unitary operation of the quantum computer.
σ_x	Pauli X -operator.

μ	Control parameter.
γ	Single parameter.
ℓ_{ij}	Distance between the quantum ports in $G_{QG}^{k,r}$.
$E_L(\vec{\Phi})$	Energy $E_L(\vec{\Phi})$ of the Hamiltonian at a system state $\vec{\Phi}$.
Δ	Separation point in $G_{QG}^{k,r}$ of the quantum circuit.
β	A physical-layer blockage in the actual layer of the quantum circuit.
\mathcal{P}	A path between the quantum ports of the quantum circuit.
$S_v(P_i)$	A vertical symmetry axis of a proximity group P_i on QG .
$x_{S_v(P_i)}$	The x -coordinate of $S_v(P_i)$.
σ_i	A cell in the grid of the quantum circuit.
x_i	A bottom-left x coordinate of a cell σ_i in the grid of the quantum circuit.
κ_i	Width of a cell σ_i in the grid of the quantum circuit.
(σ^1, σ^2)	Symmetry pair.
$\mathbf{x}_{F_1}^d$	A d -dimensional constraint vector with the symmetry considerations.
$N_{(\sigma^1, \sigma^2)}$	Number of (σ^1, σ^2) symmetry pairs in $G_{QG}^{k,r}$.
N_{σ^S}	Number of σ^S -type cells in $G_{QG}^{k,r}$.
N_{σ^0}	Number of σ^0 -type cells in $G_{QG}^{k,r}$.
r_i	Rotation angle of an i -th cell σ_i in $G_{QG}^{k,r}$.
δ_{ij}	Effective width of the quantum wire ij in the QG circuit.
$J_{\max}(T_{ref})$	Maximum allowed current density at a given reference temperature T_{ref} .
h_{nom}	A nominal layer height.
δ'_{ij}	Effective width of the quantum wire ij .
$\chi_{\varphi_{ij}}$	Maximally allowed value for the phase drops.
ℓ_{eff}	Effective length of the quantum wire, $\ell_{eff} \leq (\chi_{\varphi_{ij}} \delta_{ij}) / \psi_{ij} r_0(T_{ref})$, where $r_0(T_{ref})$ is a conductor sheet resistance.
ℓ_{ij}	Distance between the quantum ports in $G_{QG}^{k,r}$, where f_l is a cost function between the layers of the multilayer structure of QG .
$w_{QG}(k)$	Total quantum wire area of a particular net k of the QG circuit.

$\psi_{i \rightarrow j}$	Condensate wave function amplitude in direction $i \rightarrow j$ between the quantum ports.
$\psi_{j \rightarrow i}$	Condensate wave function amplitude in direction $j \rightarrow i$ between the quantum ports.
$\xi_{i \rightarrow j}$	Residual condensate wave function amplitude, $\xi_{i \rightarrow j} = \phi_{ij} - \psi_{i \rightarrow j}$, where $\phi_{ij} = \min(\psi_{i \rightarrow j} , \psi_{j \rightarrow i})$.
$\bar{\xi}_{j \rightarrow i}$	Decrement of a current wave function amplitude $\psi_{i \rightarrow j}$ for a backward direction, $j \rightarrow i$, $\bar{\xi}_{j \rightarrow i} = -\psi_{i \rightarrow j}$.
$\Gamma_{j \rightarrow i}$	A residual quantum wire length for $\bar{\xi}_{j \rightarrow i}$.
\mathcal{N}	Network of QG quantum circuit.
\mathcal{N}_R	Residual network of QG quantum circuit.
\bar{M}_{QG}	Topological map of the network \mathcal{N} .
L_c	Connection list of \mathcal{N} in QG .
\bar{M}_{QG}	Topological map of the \mathcal{N}_R residual network of QG .
\bar{L}_c	Connection list of the \mathcal{N}_R residual network of QG .
$N_{\bar{C}}$	Number of \bar{C} negative cycles in \bar{M}_{QG} .
$sn_{k,i}$	An i -th subnet of a net k of the QG quantum circuit.
\mathcal{A}_{BF}	Bellman-Ford algorithm.
\mathcal{A}_K	Kruskal algorithm.
\mathcal{T}_{QG}	Minimum spanning tree.
$S_{\mathcal{T}_{QG}}$	Set of quantum wires with $\delta_{ij} > 0$.
δ_0	Minimum width can be manufactured physically.
$d_{L1}(\cdot)$	L1-distance function.
$f_c(x, y)$	A cost function, for a quantum port pair $(x, y) \in G_{QG}^{k,r}$, defined as $f_c(x, y) = \gamma(x, y) + d_{L1}(x, y)$, where $\gamma(x, y)$ is the real path size from x to y in the multilayer grid structure $G_{QG}^{k,r}$ of QG , while $d_{L1}(x, y)$ is the L1 distance in the grid structure.
A^*	A^* search algorithm.
$\mathcal{P}^*(x, y)$	A lowest cost path between quantum ports $(x, y) \in G_{QG}^{k,r}$.